Journal of Energy Chemistry 77 (2023) 572–580

Contents lists available at ScienceDirect

Journal of Energy Chemistry

journal homepage: www.elsevier.com/locate/jechem

http://www.journals.elsevier.com/journal-of-energy-chemistry/

A stable anthraquinone-derivative cathode to develop sodium metal batteries: The role of ammoniates as electrolytes

Débora Ruiz-Martínez, José M. Orts, Roberto Gómez *

Departament de Química Física i Institut Universitari d'Electroquímica, Universitat d'Alacant, Apartat 99, Alicante E-03080, Spain

ARTICLE INFO

Article history:
Received 4 March 2022
Revised 18 November 2022
Accepted 21 November 2022
Available online 26 November 2022

Keywords:
Sodium metal batteries
Anthraquinone-based cathode
Vat dye
Indanthrone blue
Inorganic electrolytes
Liquid ammoniates

ABSTRACT

Rechargeable sodium metal batteries constitute a cost-effective option for energy storage although sodium shows some drawbacks in terms of reactivity with organic solvents and dendritic growth. Here we demonstrate that an organic dye, indanthrone blue, behaves as an efficient cathode material for the development of secondary sodium metal batteries when combined with novel inorganic electrolytes. These electrolytes are ammonia solvates, known as liquid ammoniates, which can be formulated as $NaI{\cdot}3.3NH_3$ and $NaBF_4{\cdot}2.5NH_3$. They impart excellent stability to sodium metal, and they favor sodium non-dendritic growth linked to their exceedingly high sodium ion concentration. This advantage is complemented by a high specific conductivity. The battery described here can last hundreds of cycles at 10 C while keeping a Coulombic efficiency of 99% from the first cycle. Because of the high capacity of the cathode and the superior physicochemical properties of the electrolytes, the battery can reach a specific energy value as high as 210 W h kg_{IB}^{-1}, and a high specific power of 2.2 kW kg_{IB}^{-1}, even at below room temperature (4 °C). Importantly, the battery is based on abundant and cost-effective materials, bearing promise for its application in large-scale energy storage.

1. Introduction

The demand for energy storage is on the rise in the last years due to both the increasing energy consumption and the need to satisfy it with renewable sources. There are different ways of storing energy, among which batteries offer several advantages such as high energy efficiency, fast response, flexibility, and low maintenance [1,2]. During the last decades, sodium batteries have been intensively investigated as a promising alternative to lithium batteries as sodium shows similar physicochemical properties to those of lithium and, in addition, it is a highly abundant element resulting in a lower device cost [3–6]. So far, a few sodium metal batteries (SMBs) have been commercialized, such as the Na-S battery and the ZEBRA battery. However, these operate at high temperature (300 °C or higher), which implies safety hazards. Currently, the scientific community is making great efforts to develop low- and room-temperature SMBs [7]. One of the main drawbacks of this technology is the high reactivity of sodium metal with most of the organic electrolytes together, with its dendritic plating. In this respect, over the last years, extensive studies have been carried out to optimize the electrolyte and electrode formulation, which have entailed (i) changes of salt, solvent and incorporation of additives in the electrolyte [8,9], (ii) building an artificial SEI (solid electrolyte interface) [10,11], and (iii) designing sodiophilic 3D host materials [12,13]. In this context, we have proposed that novel sodium-metal batteries could be developed using highly concentrated electrolytes based on ammonia, known as liquid ammoniates. Two of the most representative among them can be formulated as $NaI{\cdot}3.3NH_3$ and $NaBF_4{\cdot}2.5NH_3$. Their use for sustaining highly reversible and non-dendritic sodium stripping/deposition was recently uncovered [14]. These liquids show exceedingly high sodium ion concentration (>7.6 M), low viscosity, and a high specific conductivity (up to 85 mS cm^{-1} at 25 °C). In addition, they confer high stability to sodium metal. A piece of the metal does not show any sign of reactivity when stored for several weeks in the electrolyte, remaining shiny. These liquids have already shown promising results in the context of both SMBs and sodium ion batteries [15,16]. In addition, due to both the cost-effectiveness of the sodium salts employed in comparison with others such as sodium triflate or NaTFSI, and the low price of ammonia, the ammoniates are attractive electrolytes from an economic viewpoint.

* Corresponding author.
E-mail address: roberto.gomez@ua.es (R. Gómez).

https://doi.org/10.1016/j.jechem.2022.11.034

On the other hand, the development of SMBs at room and/or low temperature is not only limited by the high reactivity of sodium metal with the typical organic electrolytes, but also by the requirement of finding active cathode materials compatible with the electrolyte. In the last years, organic compounds have received great attention as they may show several advantages in comparison with inorganic compounds [17,18]. For instance, they can exhibit multielectron redox processes, thus possessing high theoretical capacities [15,19–21]. In addition, their syntheses typically do not imply high energy consumption and even they can come from natural sources [22–27]. Therefore, organic-based cathodes can be considered as eco-friendly in comparison with their inorganic-based counterparts [28–34].

A number of organic compounds have already been studied as cathode active materials [35–39]. Among them, carbonyl compounds tend to show high capacity and fast kinetics. During the charge-discharge process, each carbonyl group is reduced to form the corresponding alcoholate, and subsequently reverted to the carbonyl form [40–44]. However, the organic-based cathodes also present some limitations such as a relatively high solubility in non-aqueous solvents and low conductivity [21]. As a result, the capacity rapidly decays and the cyclability is poor. To increase the chemical and electrochemical stability of organic-based cathodes, different strategies, such as polymerization or immobilization of the organic molecule on stable conductive matrices (formed, for instance, by carbon nanotubes), have been proposed [45–49]. In addition, the carbon nanotubes constitute a conductive host offering effective pathways for electrons, and helping to overcome the low conductivity of the organic compounds [50,51].

We present here an innovative SMB concept based on both ammoniates as electrolytes and a widely available and cost-effective organic compound as a cathode active material. Specifically, we describe the use of a commercially available vat dye, indanthrone blue (IB) or Vat Blue 4 (formulated as $C_{28}H_{14}N_2O_4$), reported here for the first time as an active material in the battery context, to the best of our knowledge. In addition, it is commercially available, and no specific synthesis procedure is needed, thus avoiding in this way the use of organic solvents, in contrast to other organic-based cathodes [12,29,42,43]. The IB molecule possesses four carbonyl groups and it can thus exchange four electrons in its redox processes, achieving a theoretical capacity of 242 mA h g^{-1} [52]. The battery described here provides excellent rate performance with a specific capacity of at least 120 mA h g_{IB}^{-1} at 10 C (1.2 A g_{IB}^{-1}) over 1000 cycles, and a specific power above 2 kW kg_{IB}^{-1} at 20 °C.

2. Experimental

2.1. Preparation of the IB-based cathode

The cathode for the battery presented here was prepared by a simple solvothermal recipe, first described by Chen et al. [53], that promotes the connection through π-π interactions between IB molecules and carbon nanotubes (NTs), used as a conductive additive. The composite IB/NT has a weight ratio 7/5. Namely, 0.64 g IB and 0.46 g NTs (Sigma Aldrich, D × L 6–9 nm × 5 μm, >95%) were mixed in *N*-Methyl-2-pyrrolidone (NMP) as a solvent. The mixture was magnetically stirred under ambient conditions for at least 4 h to form a homogeneous slurry. The viscosity of the mixture increased over time to yield a paste. Then, the paste was transferred to a Teflon-lined stainless-steel autoclave and heated at 180 °C for 12 h. The IB/NT product was filtered and washed with deionized water and acetone several times. Finally, the IB/NT composite was dried in a vacuum oven at 100 °C overnight. In the cathode formulation, PVDF (10 wt%) was also used as a binder.

2.2. Characterization

The IB particles and the IB/NT composite were characterized by X-ray diffraction (XRD) using a Bruker D8 Advance, KRISTALLOFLEX K 760-80F. The morphology of the different samples was characterized by means of both field-emission scanning electron microscopy (FESEM) (ZEISS, Merlin VP Compact coupled with a EDX system Bruker Quantax 400) and transmission electron microscopy, TEM (JEOL, JEM-1400 plus).

2.3. Electrochemical measurements

All the electrochemical experiments were performed by means of a two-electrode split cell, using a Whatman 934-AH glass microfiber separator, and sodium metal foil as an anode (electrode to which all potentials are referred). The cells were assembled in a nitrogen-filled glovebox with the concentration of moisture and oxygen below 0.5 ppm. $NaI{\cdot}3.3NH_3$ and $NaBF_4{\cdot}2.5NH_3$ were used as ammonia-based electrolytes. The working electrodes were prepared by drop casting from a slurry. Typically, the IB/NT composite and the PVDF binder were mixed in a weight ratio 9:1 in NMP and the mixture was magnetically stirred for at least 4 h at room temperature to form a paste. Then, an average of 2.1 mg_{IB} cm^{-2} was deposited on a carbon-coated aluminum foil substrate, unless otherwise stated. The electrodes were dried at 60 °C overnight inside the glovebox. Cyclic voltammograms were recorded at different scan rates from 20 to 5 mV s^{-1}, and galvanostatic charge-discharge experiments were performed at different currents (C rates). Electrochemical impedance spectroscopy (EIS) measurements were conducted in the range from 100 kHz to 10 mHz using a perturbation amplitude of ±10 mV. All the electrochemical measurements were carried out using an Origalys potentiostat–galvano stat (OGF-500). The cell was located inside the glovebox when the measurements were carried out at room temperature, or in a fridge when it was measured at below-room temperature (4 °C).

3. Results and discussion

The molecular structure of IB is depicted in Fig. 1(a). As observed, full sodiation of the IB molecule implies the exchange of 4 electrons and the reduction of its four carbonyl groups. Fig. 1(b) shows the XRD pattern, which resembles that of the anthraquinone crystals. It is characterized by relatively broad reflections, indicating that the IB molecules form molecular crystals with a rather low degree of crystallinity. The diffraction peaks at 10°–15° and 25°–30° are presumably due to the π-π stacking of the aromatic moieties [54]. Fig. 1(c) shows representative electron microscopy (FESEM and TEM) images for IB samples, in which the crystals show a needle-like elongated shape with lengths from 0.5 to 1 μm and diameters around 100 nm (up to 200 nm in some cases).

Fig. 2(a) shows the XRD patterns for the IB/NT composite together with those of the carbon NTs and the IB sample for the sake of comparison. The carbon NT diffractogram shows a broad peak at 25° [55]. The diffractogram for the composite shows much sharper IB reflections than that of the untreated IB sample, which indicates the formation of IB crystals with a high degree of crystallinity, together with a broad signal at around 25° coming from the NTs and seen as a deviation of the baseline. Fig. 2(b) shows SEM images for the IB/NT composite confirming that the IB particles are well dispersed with the carbon NTs after the solvothermal synthesis [56]. Importantly, the IB crystals have now a much sharper size distribution, with an average length of 2 μm and diameters ranging from 150 to 200 nm. There is thus a significant increase in crystal size upon the solvothermal treatment, which indicates that

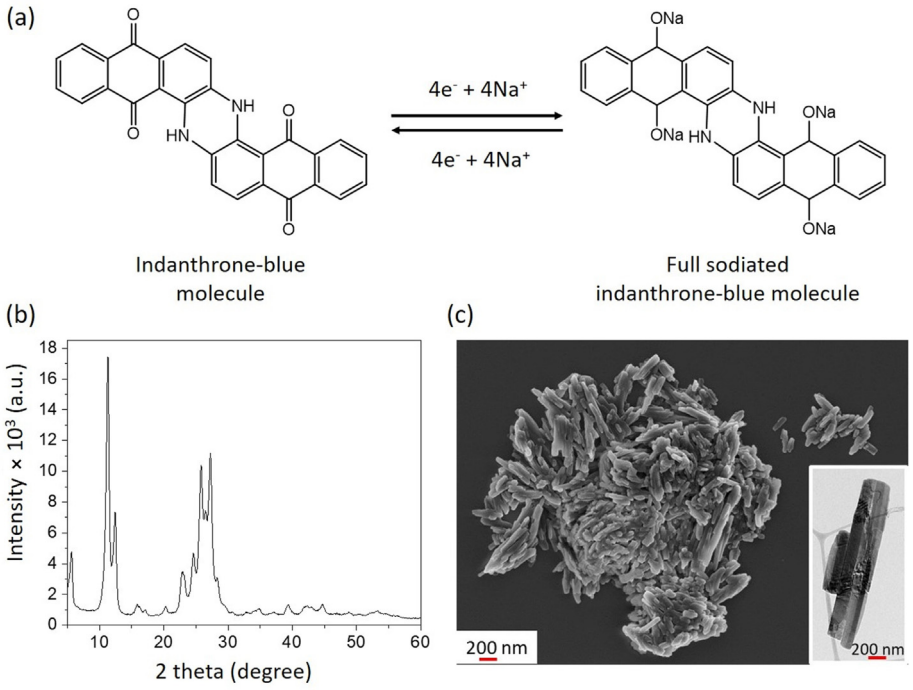

Fig. 1. Redox process showing the structure of the indanthrone-blue molecule prior and after being sodiated (a), XRD pattern for the IB powder (b), and representative FESEM image for the IB powder (c). Inset in (c): TEM image in which the crystal morphology is clearly defined.

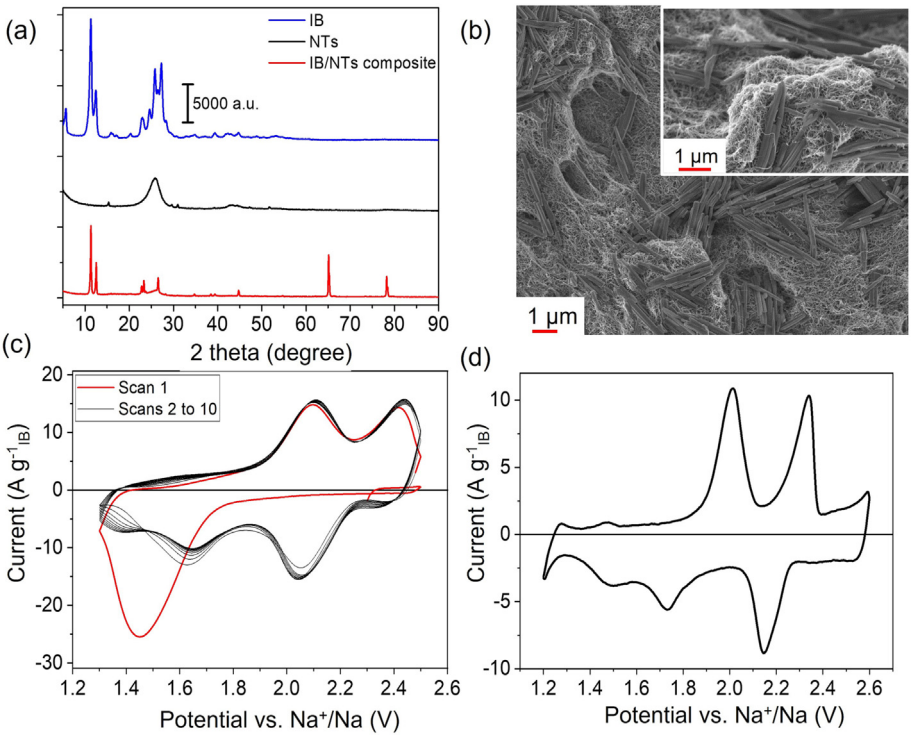

Fig. 2. XRD pattern for the IB/NT composite, the carbon NTs, and an untreated IB sample (a), FESEM images for the IB/NT composite (b), initial CVs for an IB electrode (IB/NTs (7/5):PVDF 90:10) at 20 mV s^{-1} in NaI·3.3NH_3 (red curve corresponds to the first cycle) (c), and stationary CV for an IB electrode (IB/NTs(7/5):PVDF 90:10) at 5 mV s^{-1} in NaI·3.3NH_3 (d).

it does not only lead to a well-dispersed mixture, but also to IB recrystallization. This, in turn, would explain the sharpening of the IB diffractogram.

The IB-based cathode was engineered using PVDF as a binder in the formulation to obtain an IB/NT(7/5):PVDF 90:10 electrode composition. The electrochemical characterization was performed in a two-electrode split cell using Na metal foil as an anode and NaI·3.3NH_3 as an electrolyte. Fig. 2(c) shows the initial and several subsequent cyclic voltammograms (CVs) for an IB/NT(7/5):PVDF 90:10 electrode at 20 mV s^{-1}. The first cycle (CV in red) shows a

wide peak at 1.45 V, which disappears in the subsequent scans. This could be considered as an activation process for the IB electrode, as reported by other authors [54,57–59]. It is likely related to a sodium transport barrier that there exists for the first electrode sodiation, associated with achieving the wetting of the IB particles in the inner part of the film. The electrode wetting would be attained to a great extent during the first negative-going voltammetric scan, which also leads to cathode sodiation. From scan 2 on, two anodic and three cathodic voltammetric peaks can be distinguished for the redox response of the IB molecule. The redox processes observed in the negative-going scan correspond to the reduction of C=O groups of the IB molecule to C–ONa. The reoxidation of C–ONa to C=O takes place in the subsequent positive-going scan. The stationary CV recorded at 5 mV s^{-1} clearly demonstrates that the charge storage mechanism for the IB electrode is predominantly Faradaic in nature (Fig. 2d) [58]. Note that the peak potentials have slightly changed with respect to those in Fig. 2(d), because different scan rates were used in each case.

With the aim to determine the maximum capacity and the operative potential window for the IB electrode, a series of CVs was recorded for different values of the negative potential limit (see Fig. S1). The cathodic charge (Q_-) was then evaluated for each voltammogram by integrating the area under the curve. In the potential window between 0.4 and 2.6 V, it was found that full sodiation of the IB sample likely takes place as the theoretical capacity of 242 mA h g^{-1} for IB is achieved. However, full sodiation of the IB electrode leads to a significant mechanical destabilization of the electrode, resulting in partial delamination of the active material film from the substrate, which is probably related with large volume changes of the IB particles upon cycling [19,40,60]. Such a volume change is probably accompanied with partial dissolution/recrystallization of the IB particles, whose size distribution and morphology experience a significant change. Aiming to mitigate this drawback, charge-discharge experiments were limited to the window between 1.3 and 2.5 V vs Na^+/Na, which sacrifices half of the gravimetric capacity, but it strongly increases IB stability. Furthermore, the effect of the window narrowing on the specific energy is relatively minor.

Fig. 3(a and b) shows a comparison of the CVs at 20 mV s^{-1} in the sodium ammoniate electrolyte for IB-based and AQ-based electrodes (AQ: 9,10-anthraquinone). As expected, the electrodes show similar electrochemical behavior as both active materials have an anthraquinoid structure. There exist some differences, though, related to the fact that each molecule has different substituents in the condensed rings [22]. The CVs for both AQ and IB show two anodic redox peaks. However, while for the AQ electrode, there are two cathodic peaks, in the case of IB, three cathodic peaks are clearly distinguished (at 2.0, 1.60 and 1.35 V). As shown in Fig. S2, the charge under the IB reduction peaks at 1.60 and 1.35 V (blue colored area) is approximately the same as under the peak at 2.0 V (orange colored area). It is thus likely that the anodic peak at 2.15 V corresponds to the cathodic peaks at 1.35 and 1.60 V, while the anodic peak at 2.45 V is associated with that at 2.00 V. As observed, the voltammetric response for the AQ electrode is better defined, which is probably linked to the simpler structure of the electroactive compound. The higher complexity of the IB molecule could underlie the appearance of three reduction peaks in Fig. 3(a). As more sodium enters the electrode to counterbalance the negative charges in the alcoholates being produced, kinetic barriers would appear, which would be at the origin of the splitting of one of the reduction peaks. In any case, the potential separation between the two quasi-reversible redox processes in both cases can be attributed to a larger Coulombic or steric repulsion for the incorporation of the second Na^+ ion within the same anthraquinone unit [61,62]. From the comparison of the CVs in Fig. 3(a and b), it can be concluded that the redox process at more positive potentials is kinetically more favorable for IB than for AQ, as the separation of the anodic and cathodic peak potentials is smaller by 0.1 V, while the redox process at less positive potentials is more sluggish in the case of IB.

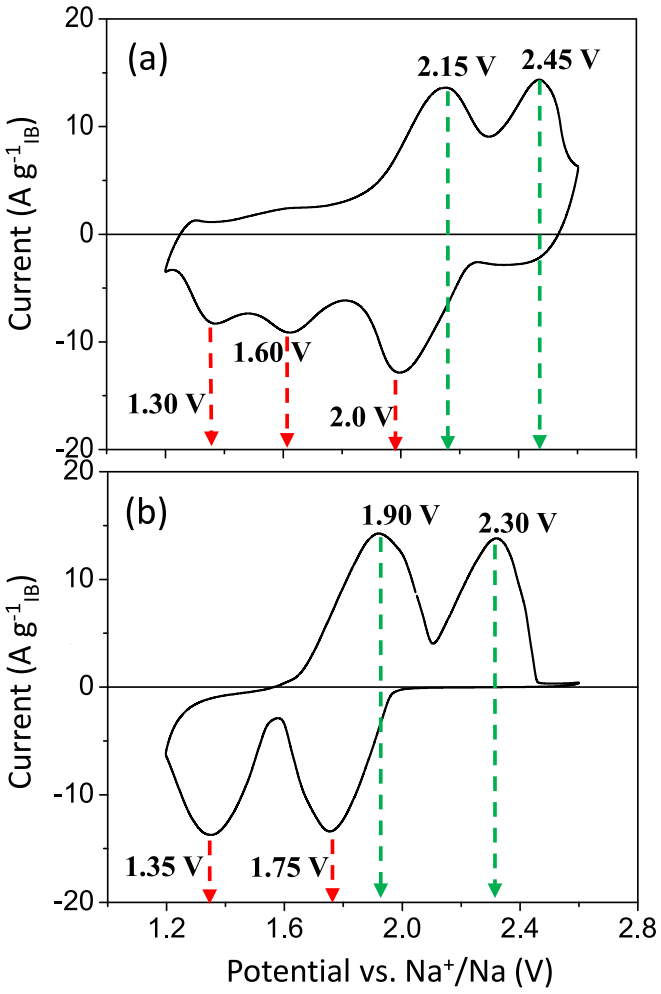

Fig. 3. Cyclic voltammograms at 20 mV s^{-1} in NaI·3.3NH_3 for the electrodes IB/NT:PVDF (60:30:10) (a), and AQ/NT:PVDF (60:30:10) (b).

To achieve the maximum performance of the IB-based cathode, a preliminary optimization of the electrode composition was carried out. Attention was paid to both the type of conductive additive (carbon NTs or carbon Super P) and the type of binder (PVDF, PTFE or Na-CMC). The mass fraction of NTs in the electrode formulation was also relevant in this study, as well as the procedure followed to mix IB particles and additives. Further information on the electrochemical behavior for each cathode composition can be found in the SM (Figs. S3 and S4). After the optimization process, the formulation IB/NT(7/5):PVDF 90:10 was chosen as the most promising.

Fig. 4(a) shows some of the initial ten consecutive charge-discharge curves at 10 C for a Na|NaI·3.3NH_3|IB battery at 4 °C. They are characterized by two plateaus in both the charge and the discharge, which are related to the peaks observed in the CVs. The gravimetric capacity of the electrode has a value of 120 mA h g_{IB}^{-1}, keeping a Coulombic efficiency of 99%. In addition, an estimate of the energy efficiency leads to a value of 92% for a system based on IB and NaI·3.3NH_3 at 4 °C, which is significantly higher than the values reported for related systems at room temperature [21,58,63]. The energy efficiency has been calculated as the ratio between the average discharge and charge voltages [64]. The excellent electrochemical behavior and the high energy efficiency

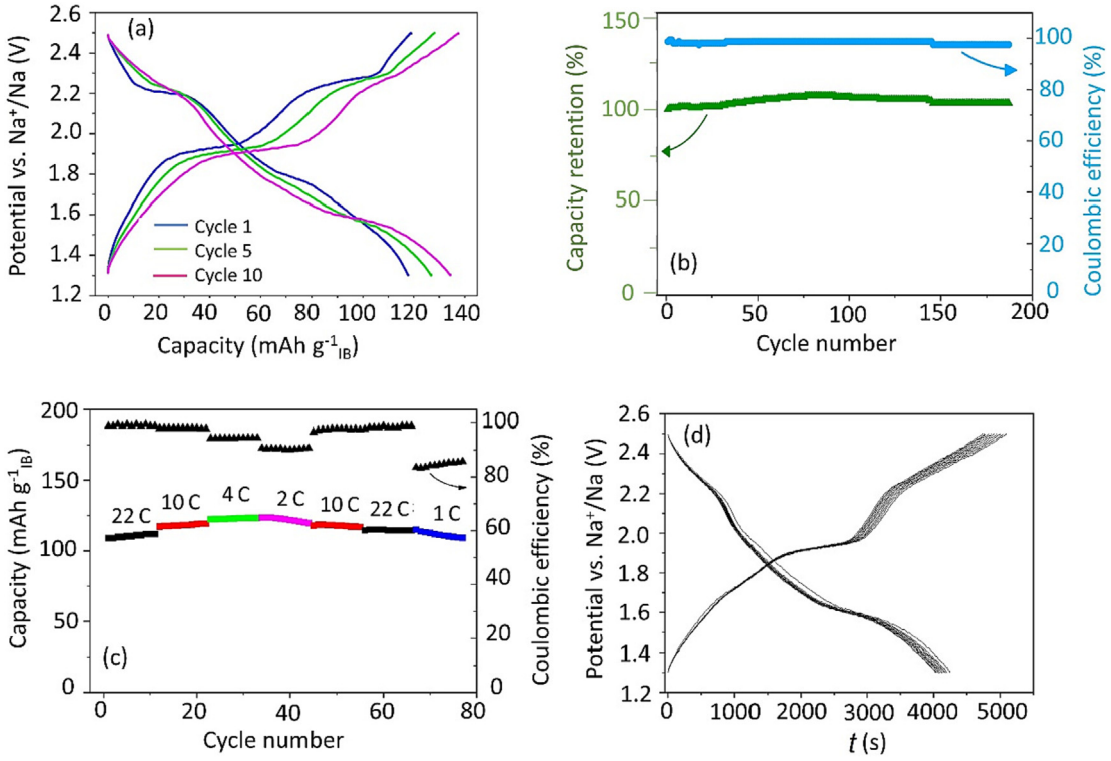

Fig. 4. The 1st, 5th and 10th charge-discharge cycles for an IB electrode (IB/NT(7/5):PVDF 90:10) in NaI·3.3NH_3 at 1.1 A g_{IB}^{-1} (a), gravimetric capacity retention and Coulombic efficiency for an IB electrode at 2.4 A g_{IB}^{-1} (b), gravimetric capacity and Coulombic efficiency for an IB electrode at different C rates (c), and charge-discharge cycles for an IB electrode (IB/NT(7/5):PVDF 90:10) at 0.1 A g_{IB}^{-1} (d).

obtained for this battery are directly connected to using a liquid ammoniate as an electrolyte. It should be stressed that this performance is achieved at 4 °C, enabled by the high specific conductivity of the liquid ammoniate, even at below-room temperatures [14].

Fig. 4(b) shows that the capacity retention is remarkable for 200 cycles, while the Coulombic efficiency is 99%. These results have been obtained at a fast charge-discharge rate (2.4 A g_{IB}^{-1}). These data highlight the advantages of the liquid ammoniate as an electrolyte for SMBs, because even operated at high current densities, the cell does not short internally. This is directly connected to the non-dendritic growth of sodium in this electrolyte [45].

Fig. 4(c) shows the evolution of the specific capacity of the Na|NaI·3.3NH_3|IB system for several C rates. Initial cycling has a favorable effect on capacity as concluded from the values obtained prior to cycling and after 60 cycles at 22 C (see below). On the other hand, a slight increase in capacity is observed for low C rates. Usually, lower C rates allow for more extensive Na^+ intercalation and, therefore, there is a better use of the active material. However, a rate of 2 C does not trigger an increase in the IB electrode capacity compared with a rate of 4 C because the electrode has already attained its maximum theoretical capacity assuming the exchange of $2e^-$ per molecule (121 mA h g_{IB}^{-1}) in the potential range being used. As observed, for a rate of 1 C, both the gravimetric capacity and the Coulombic efficiency significantly decrease, suggesting the existence of a parasitic reaction during charging. The diminution of the Coulombic efficiency is already discernible at 4 C. This is clearly shown in Fig. 4(d), which displays an extra time in the potential vs *t* plot at 0.1 A g_{IB}^{-1} during the charge process, implying overoxidation at the cathode.

As commented previously, volume changes during cycling could lead to a partial delamination of the IB film and to exposure of the substrate, which could get oxidized (corroded) during the charge process (see Figs. S5 and S6). Further work is ongoing to both clarify the origin of this problem and find the way to overcome it. In any case, the capacity reached for the IB electrode in NaI·3.3NH_3 is comparable with that for other related systems based on organic electrolytes, less cost-effective than NaI·3.3NH_3 [50,58,65].

The long-term stability of the Na|NaI·3.3NH_3|IB system was tested at 10 C between 1.3 and 2.6 V. The active material loading was 1.4 mg_{IB} cm^{-2} instead of the 2.1 mg_{IB} cm^{-2} employed in previous experiments to both improve the mechanical stability of the working electrode and show the effect of the mass loading on the electrode performance. Fig. 5(a) illustrates the cyclability at 10 C for an IB electrode that shows an initial discharge capacity of 110 mA h g_{IB}^{-1} which increases gradually during the initial 25 cycles up to a value of 125 mA h g_{IB}^{-1}. This capacity enhancement can also be considered as an activation process for the IB electrode, as reported by other authors [54,57–59]. Such a process is likely related to an increase of the interfacial area of the electrode caused by a progressive wetting of the IB particles in the inner part of the film. The capacity is stable until cycle 100–150 and then it starts decreasing. A sharp small drop can be seen at around 500 cycles (a similar behavior was observed in Fig. 4(b) after 150 cycles), which is probably related to a partial loss of contact among the particles and/or between the particles and the substrate due to the size and morphological changes of the IB particles during cycling. In any case, the IB electrode achieves 1000 charge-discharge cycles while retaining a 67% of its maximum capacity even when using high C rates [50,51,54]. In addition, the data obtained during the charge/discharge cycles indicate that this battery can attain values for the specific energy and specific power as high as of 210 Wh kg_{IB}^{-1} and 2200 W kg_{IB}^{-1}, respectively, maintaining a Coulombic efficiency of 99% along the experiment. It is worth noting that the capacity reached for the IB electrode in NaI·3.3NH_3 is comparable with that for other systems based on organic electrolytes less cost-effective than NaI·3.3NH_3 [50,58,65]. It is important to highlight the use of

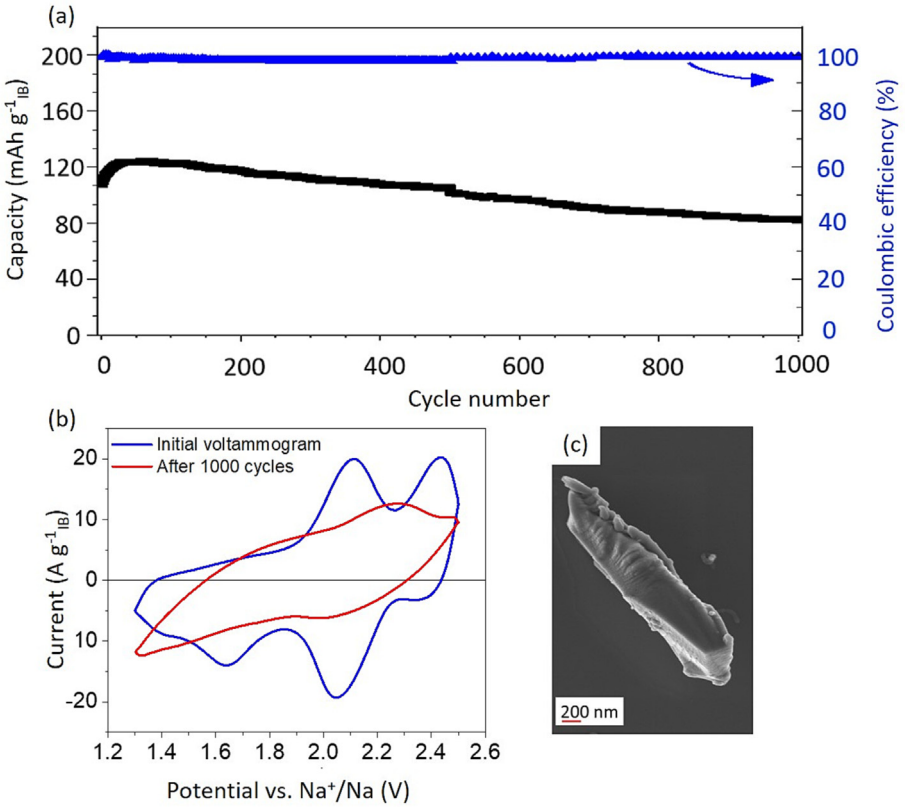

Fig. 5. Gravimetric capacity vs number of cycles for an IB electrode (IB/NT(7/5):PVDF 90:10) in NaI·3.3NH_3 at 10 C (a), CVs at 20 mV s^{-1} for an IB electrode before (blue) and after (red) 1000 charge-discharge cycles (b), and SEM image of a representative IB particle after 1000 charge-discharge cycles (c).

NaI·3.3NH_3 as an electrolyte for SMBs, as it enables applying high C rates while keeping high specific capacities, energy and power densities, and Coulombic efficiencies thanks to its very high values of sodium concentration and specific conductivity.

Fig. 5(b) shows CVs for an IB-based electrode before and after 1000 charge-discharge cycles. The morphology of the CV was strongly affected by cycling and the characteristic redox peaks for IB are no longer distinguishable. The existence of a substantial series resistance (slope of the CV) is also apparent, which is likely related to the loss of contact between substrate and active material referred to above. Fig. 5(c) shows a representative SEM image for an IB particle after 1000 charge-discharge cycles. As deduced from a comparison of Fig. 5(c) and 1(c), upon cycling, there is a significant increase in particle size, which is probably connected to the capacity loss and the delamination of the electrode active material from the substrate.

The possibility that the reduced IB species becomes partly dissolved in the electrolyte cannot be discarded. In this respect, a very slow discharge of the IB electrode at 20 μA cm^{-2} was carried out in a three-electrode cell using two Na metal pieces as reference and counter electrodes in NaI·3.3NH_3. After the discharge of the electrode down to 1.3 V, just a very slight electrolyte coloring was observed (see Fig. S7). This experiment confirms the very low solubility of the reduced IB species, indicating that the capacity decay is not mainly due to a dissolution of the active material during cycling, but to film delamination and particle detachment, associated with the large volume changes of the IB particles.

Fig. 6(a) shows the Nyquist plots obtained after the IB-based battery was submitted to different numbers of cycles. The impedance spectra are characterized by a relatively well-defined semicircle in the high frequency range and by a line with a slope well above one in the low frequency range. The behavior observed at low frequencies does not seem to be mainly related to the Warburg element (processes under diffusion control), but rather to a pseudo-capacitive behavior [66,67]. Some minor changes of the semicircle radius are observed with the number of charge-discharge cycles. After 50 cycles, the radius diminishes, followed by a progressive increase after 100 and 150 cycles. In the latter case, two semicircles can be discerned in the high frequency region. At very high frequencies, complex impedance appears in the second quadrant, indicating the existence of an inductive contribution, probably coming from cell connections. In any case, the stability of the electrochemical impedance spectra upon 150 cycles is remarkable, indicating that no significant degradation of the IB cathode occurs.

Fig. 6(b) shows a simple equivalent circuit that allowed us to obtain quantitative information for the interpretation and discussion of the EIS (by employing the software *EIS Spectrum Analyser* [68]). The circuit is composed of six elements: (i) L1, which is an inductance, likely related to cell connections; (ii) R1, which corresponds to the electrolyte resistance; (iii) R2 associated with the charge transfer resistance at the Na electrode; (iv) CPE1 and CPE2 are the constant phase element for the Na and IB electrodes, respectively. Finally, W1 is the Warburg element representing Na^+ diffusion within the cathode. Another charge transfer resistance was initially included in series with W, but EIS simulation and fitting showed that its contribution to the spectra was negligible. The proposed circuit allows for a satisfactory fit of the experimental EIS data as can be seen in Fig. S8. The parameters resulting from the fitting are gathered in Table S1. It is worth noting that the elements L1, R1, and CPE1 do not change with the number of cycles, which supports that they are assigned to contacts, electrolyte, and Na electrode. However, R2 grows slightly with the number of cycles, from 3.5 Ω cm^2 initially to 4.4 Ω cm^2 after 250 cycles. Spectra sim-

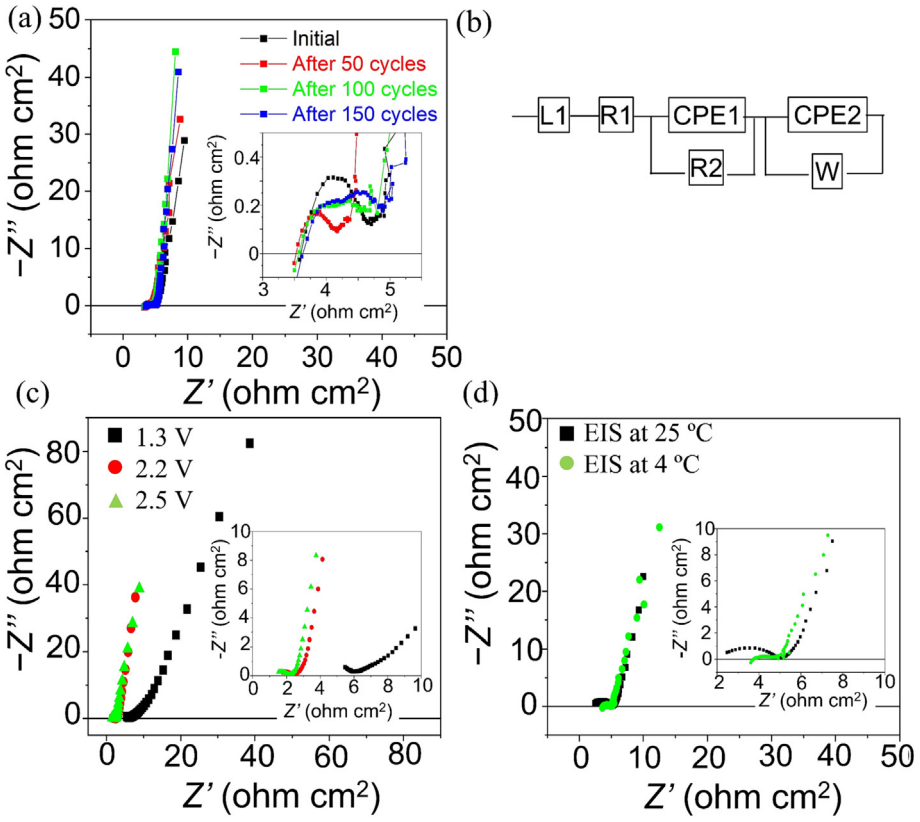

Fig. 6. Nyquist plots for an IB (IB/NTs(7/5):PVDF 90:10) electrode in NaI·3.3NH_3 in the frequency range from 100 kHz to 10 mHz at 2.2 V, initially and upon the application of different number of cycles (a), equivalent electric circuit used for analyzing the experimental spectra (b), Nyquist plots for the IB electrode in NaI·3.3NH_3 at different applied voltages (c) and at 2.2 V at 25 °C and 4 °C (d). Insets in (a), (c), and (d): details of the high frequency region.

ulation shows that the low frequency region is dominated by CPE2 rather than by W1. It is worth noting that the exponent that characterizes the CPE2 impedance, n_{CPE2}, (see Table S1) is initially as high as 0.91 and it even increases to 0.95 after 100 cycles. These values indicate that CPE2 can be considered a quasi-ideal capacitor, particularly after 100–150 cycles. It is also interesting to point out that the overall appearance of the Nyquist plots in Fig. 6(a) is close to that of a capacitor, while those obtained for systems based on common organic electrolytes [35,50,56,69] have a more important resistive component. These results and the general features of the EIS indicate that the NaI·3.3NH_3 is a superior electrolyte to develop sodium metal batteries.

On the other hand, due to the large morphological changes that the IB particles suffer upon cycling and the ensuing expected change in the electrode structure, the Nyquist plot is markedly different after 1000 charge-discharge cycles, indicating a dramatic increase of resistive contributions (see Fig. S9).

Admittedly, the EIS data could be fitted to other more elaborated circuits with elements capturing more precisely the nature of the electrode. In this respect, several models have been considered for porous electrodes [70]. The electrodes typically employed in batteries should not be considered as composed of pores of equal size. For instance, models based on capacitive pore walls, assuming a lognormal pore radius distribution with constant pore volume leads to Nyquist plots virtually identical to those shown in Fig. 6(a). Accepting such a model [71] one can interpret the way in which the low frequency region evolves with the number of cycles. The fact that upon 100–150 cycles the straight line observed at low frequencies is more vertical would mean that the radius distribution gets narrower. The initial effect of the charge/discharge cycles would thus be to homogenize the particle and pore size, which, on the other hand, is also reflected in an increase in the gravimetric capacity.

EIS experiments were also performed for applied potentials of 1.3 and 2.6 V with the aim of testing the effect of the state of charge on the electrode–electrolyte interphase. In this way, at 1.3 V the IB electrode is completely discharged, while at 2.6 V, it is fully charged. The open circuit potential of the battery is around 2.2 V, being the IB electrode mainly in its oxidized state. As observed in Fig. 6(c), at 1.3 V the Nyquist plot shifts to higher impedance values and a flattened high-frequency semicircle can be clearly distinguished. In addition, the slope observed in the linear region at low frequencies is lower, indicating an evolution in the character of the CPE2 element, which would change from an almost purely capacitive character to a more resistive behavior. This result agrees with the fact that, at 1.3 V, the electrode is sodiated and the capacitance is low as deduced from the CV in Fig. 3(a). As the capacitive component of the CPE diminishes, the overall CPE behavior is more resistive.

One of the potential advantages of the ammoniate electrolytes is that they could be employed favorably at below-room temperatures. For illustrating this aspect, electrochemical impedance spectra were also acquired at 4 °C. Fig. 6(d) shows Nyquist plots for the battery Na|NaI·3.3NH_3|IB/NT(7/5):PVDF 90:10 at 4 and 25 °C for the sake of comparison. As expected, temperature does not alter in a significant way the Nyquist plots. In particular, the close-to-capacitive behavior observed in the low frequency region is virtually the same in both cases. This is coherent with the fact that the specific capacity attained by the cathode is the same regardless of the temperature value (Fig. S9).

The following results point to the fact that other liquid ammoniates may also have an excellent behavior as electrolytes for

SMBs. Specifically, experiments with the IB electrode (IB/NTs(7/5): PVDF 90:10) were also carried out in the sodium tetrafluoroborate ammoniate ($NaBF_4{\cdot}2.5NH_3$). The use of this alternative ammoniate is interesting as $NaBF_4$ is markedly more cost-effective than NaI and it may potentially lead to systems with voltage windows wider than for the NaI ammoniate.

Fig. 7(a) shows a stationary voltammogram at 5 mV s^{-1} obtained after stabilization of the electrode (by performing ten cycles at 20 mV s^{-1}). Three anodic peaks can be distinguished at 1.6, 2.5 and 2.9 V as well as four cathodic peaks at 2.6, 1.75, 1.55 and 1.2 V vs Na^+/Na. The fact that three redox peaks are observed in the working potential window suggests that three distinct sodiation processes of the IB may be occurring, although additional experimental or theoretical information is needed to clarify this question. In addition, the IB redox peaks appear at more positive potential than for an analogous experiment in $NaI{\cdot}3.3NH_3$ (see Fig. 3a). This indicates that the tetrafluoroborate anion can stabilize the sodiated IB electrode to a larger extent than iodide does. Such stabilization could come from the ability of tetrafluoroborate anions to favorably interact simultaneously with the sodium cation and the NH moieties in the dye molecule. On the other, the high concentration of ions in the electrolyte and the relatively low dielectric constant of ammonia should favor the formation of ionic pairs in the electrolyte. In fact, the formation of aggregates between sodium and tetrafluoroborate in ionic liquids has been reported [72]. In any case, these observations point to the possibility of designing higher energy density devices using the $NaBF_4$-based electrolyte.

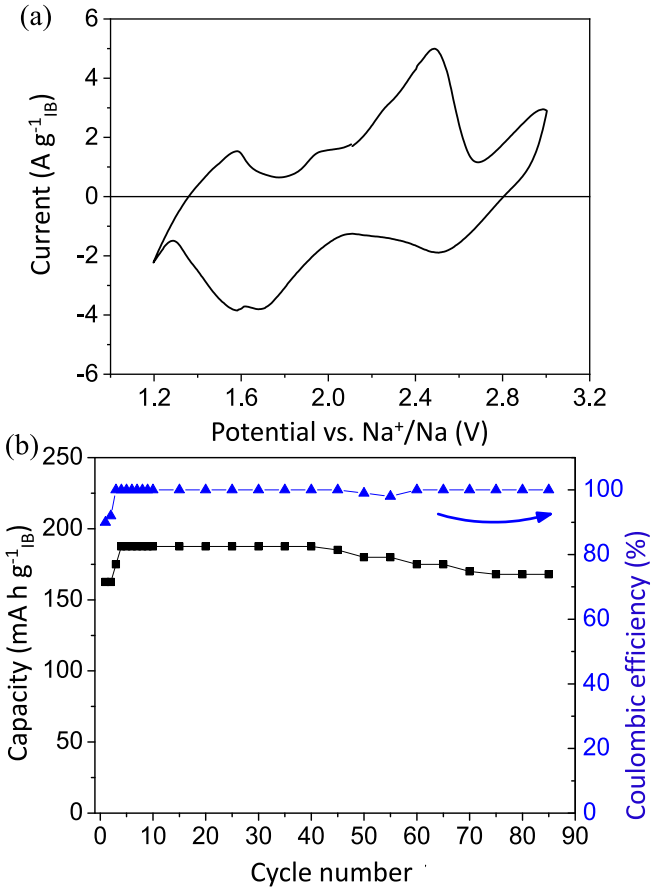

Fig. 7. Electrochemical behavior of an IB-based electrode in $NaBF_4{\cdot}2.5NH_3$ evaluated through a CV at 5 mV s^{-1} (after ten cycles at 20 mV s^{-1}) (a), and charge-discharge cycles at 8 C (2.3 mA cm^{-2}) (b). The experiments were performed in a two-electrode split cell at 4 °C using a Na metal piece as a counter electrode.

Fig. 7(b) displays several charge-discharge cycles for an IB electrode at 8 C in the $NaBF_4{\cdot}2.5NH_3$ electrolyte. It shows an initial discharge capacity of 163 mA h g_{IB}^{-1} and it reaches its maximum value of 188 mA h g_{IB}^{-1} after only 5 cycles. The electrochemical behavior of this battery is nearly stable for close to 90 cycles, retaining a 90% of its maximum capacity at the end of the cycling. These values are consistently larger than for the NaI ammoniate. This fact is related to the wider potential window employed in this experiment (0.3 V wider than for the NaI ammoniate), allowing for a higher average number of electrons exchanged per dye molecule. Other factors that may contribute to the enhanced capacity are the higher (i) specific conductivity of $NaBF_4{\cdot}2.5NH_3$ (70 mS cm^{-1} vs. 55 mS cm^{-1} for $NaI{\cdot}3.3NH_3$, both at 4 °C) and (ii) sodium ion concentration (8.7 M vs 7.6 M). Probably, the tetrafluoroborate-induced stabilization of the sodiated dye contributes to a more extensive utilization of the active material in the cathode. The apparently shorter activation process in this electrolyte is a result of the longer system conditioning applied prior to the charge/discharge cycles (see the SM for further details).

Finally, it is worth noting that the $NaBF_4{\cdot}2.5NH_3$ electrolyte is not only cost-effective in comparison with the NaI ammoniate, but also in comparison with conventional organic electrolytes (cheaper roughly by a factor of 5). Admittedly, the use of this ammoniate presents a constraint due to its high vapor pressure at room temperature. Studies on electrolyte modification to mitigate this risk are underway in our laboratory.

4. Conclusions

This work reports on the use of an easily available and cost-effective organic vat dye as a cathode material to develop sodium metal batteries based on liquid ammoniates as electrolytes. These electrolytes show several advantages such as high ionic conductivity, cost-effectiveness in comparison with organic and ionic liquids, and low flammability. Indanthrone blue has also been shown to present several advantages such as a high theoretical capacity, cost-effectiveness, and non-toxicity. In addition, the quinone groups in the IB molecule are chemically labile, and the activation process takes place largely during the first discharge. The redox processes of an IB electrode in the liquid ammoniates used here ($NaI{\cdot}3.3NH_3$ and $NaBF_4{\cdot}2.5NH_3$) show a rather reversible behavior, even at high C rates, which is not only due to their relatively fast kinetics, but also to the fact that the electrolytes have exceedingly high sodium ion concentration and specific conductivity (even at low temperature). As a result, the use of rates as high as 2.5 A g_{IB}^{-1} does not cause a significant depletion of Na^+ in the porous structure of the electrode. This feature could enable the development of novel devices with high energy and power densities.

The experiments indicate that achieving IB full reduction requires applying potentials as low as 0.4 V. This involves considerable mechanical destabilization of the IB electrode, probably due to large volume changes during Na intercalation–deintercalation. By setting the negative potential limit at 1.3 V, an IB electrode can perform at least 1000 charge-discharge cycles at 10 C (1.8 A g_{IB}^{-1}), retaining 67% of its maximum capacity at the end of the cycling with a Coulombic efficiency of 99%. In addition, the Na|$NaI{\cdot}3.3NH_3$|IB system is characterized by specific energy and specific power values of around 210 W h kg_{IB}^{-1} and 2200 W kg_{IB}^{-1}, respectively, comparable to those of Li-ion analogous systems [21,37,50,51,63].

In summary, through a combination of IB as an active cathode material, liquid ammoniates as electrolytes and sodium metal anodes, new room temperature rechargeable sodium metal batteries can be devised, which can be from 3 to 5 times more cost-effective (materials-wise) than those based on conventional organic electrolytes or ionic liquids.

Declaration of competing interest

The authors declare that they have no known competing financial interests or personal relationships that could have appeared to influence the work reported in this paper.

Acknowledgments

This work has been developed in the context of project RTI2018–102061–B–I00 financed by FEDER/Ministerio de Ciencia e Innovación-Agencia Estatal de Investigación. The Generalitat Valenciana through project PROMETEO/2020/089 is also gratefully acknowledged. We are thankful to Dr. T. Lana-Villarreal and A. Kovacs for fruitful discussions.

Appendix A. Supplementary material

Supplementary data to this article can be found online at https://doi.org/10.1016/j.jechem.2022.11.034.

References

[1] H. Pan, Y.-S. Hu, L. Chen, Energy Environ. Sci. 6 (2013) 2338.
[2] J.-Y. Hwang, S.-T. Myung, Y.-K. Sun, Chem. Soc. Rev. 46 (2017) 3529–3614.
[3] S.M. Kimball, Mineral Commodities Summaries, U.S. Geological Survey, Reston, 2016.
[4] P.K. Nayak, L. Yang, W. Brehm, P. Adelhelm, Angew. Chemie - Int. Ed. 57 (2018) 102–120.
[5] X. Zheng, C. Bommier, W. Luo, L. Jiang, Y. Hao, Y. Huang, Energy Storage Mater. 16 (2019) 6–23.
[6] K. Chayambuka, G. Mulder, D.L. Danilov, P.H.L. Notten, Adv. Energy Mater. 8 (2018) 1800079.
[7] G.G. Eshetu, M. Martinez-Ibañez, E. Sánchez-Diez, I. Gracia, C. Li, L.M. Rodriguez-Martinez, T. Rojo, H. Zhang, M. Armand, Chem. - An Asian J. 13 (2018) 2770–2780.
[8] Y.S. Hu, Y. Lu, ACS Energy Lett. 5 (2020) 3633–3636.
[9] X. Chen, X. Shen, T.-Z. Hou, R. Zhang, H.-J. Peng, Q. Zhang, Chem 6 (2020) 2242–2256.
[10] B. Sun, P. Xiong, U. Maitra, D. Langsdorf, K. Yan, C. Wang, J. Janek, D. Schröder, G. Wang, Adv. Mater. 32 (2020) 1903891.
[11] W. Liu, P. Liu, D. Mitlin, Adv. Energy Mater. 10 (2020) 2002297.
[12] B. Liu, D. Lei, J. Wang, Q. Zhang, Y. Zhang, W. He, H. Zheng, B. Sa, Q. Xie, D.-L. Peng, B. Qu, Nano Res. 13 (2020) 2136–2142.
[13] W. Zhao, M. Guo, Z. Zuo, X. Zhao, H. Dou, Y. Zhang, S. Li, Z. Wu, Y. Shi, Z. Ma, X. Yang, Engineering 11 (2022) 87–94.
[14] D. Ruiz-Martínez, A. Kovacs, R. Gómez, Energy Environ. Sci. 10 (2017) 1936–1941.
[15] D. Ruiz-Martínez, T. Lana-Villarreal, R. Gómez, ACS Appl. Energy Mater. 4 (2021) 6806–6814.
[16] D. Ruiz-Martínez, R. Gómez, Energy Storage Mater. 22 (2019) 424–432.
[17] Y. Sun, S. Guo, H. Zhou, Adv. Energy Mater. 9 (2018) 1800212.
[18] H.G. Wang, X.B. Zhang, Chem. - A Eur. J. 24 (2018) 18235–18245.
[19] Q. Zhao, Y. Lu, J. Chen, Adv. Energy Mater. 7 (2017) 1601792.
[20] A. Vizintin, J. Bitenc, A. Kopač Lautar, K. Pirnat, J. Grdadolnik, J. Stare, A. Randon-Vitanova, R. Dominko, Nat. Commun. 9 (2018) 661.
[21] C. Yuan, Q. Wu, Q. Shao, Q. Li, B. Gao, Q. Duan, H.G. Wang, J. Colloid Interface Sci. 517 (2018) 72–79.
[22] M. Miroshnikov, K.P. Divya, G. Babu, A. Meiyazhagan, L.M.R. Arava, P.M. Ajayan, G. John, J. Mater. Chem. A 4 (2016) 12370–12386.
[23] K. Sakaushi, M. Antonietti, Acc. Chem. Res. 48 (2015) 1591–1600.
[24] H. Zhu, J. Yin, X. Zhao, C. Wang, X. Yang, Chem. Commun. 51 (2015) 14708–14711.
[25] T. Sun, Z. Li, H. Wang, D. Bao, F. Meng, X. Zhang, Angew. Chemie 128 (2016) 10820–10824.
[26] Y.H. Zhu, X. Yang, D. Bao, X.F. Bie, T. Sun, S. Wang, Y.S. Jiang, X.B. Zhang, J.M. Yan, Q. Jiang, Joule 2 (2018) 736–746.
[27] T. Sun, Z.J. Li, X.B. Zhang, Research 2018 (2018) 1936735.
[28] Y. Cao, L. Xiao, W. Wang, D. Choi, Z. Nie, J. Yu, L.V. Saraf, Z. Yang, J. Liu, Adv. Mater. 23 (2011) 3155–3160.
[29] X. Wu, W. Deng, J. Qian, Y. Cao, X. Ai, H. Yang, J. Mater. Chem. A 1 (2013) 10130–10134.
[30] T. Jin, Y. Liu, Y. Li, K. Cao, X. Wang, L. Jiao, Adv. Energy Mater. 7 (2017) 1700087.
[31] W.J. Li, S.L. Chou, J.Z. Wang, J.L. Wang, Q.F. Gu, H.K. Liu, S.X. Dou, Nano Energy 13 (2015) 200–207.
[32] S. Wang, X.B. Zhang, Adv. Mater. 31 (2019) 1805432.
[33] Y.H. Zhu, Y. Bin Yin, X. Yang, T. Sun, S. Wang, Y.S. Jiang, J.M. Yan, X.B. Zhang, Angew. Chemie - Int. Ed. 56 (2017) 7881–7885.
[34] Y.H. Zhu, Q. Zhang, X. Yang, E.Y. Zhao, T. Sun, X.B. Zhang, S. Wang, X.Q. Yu, J.M. Yan, Q. Jiang, Chem 5 (2019) 168–179.
[35] A. Ahmad, Q. Meng, S. Melhi, L. Mao, M. Zhang, B.H. Han, K. Lu, Z. Wei, Electrochim. Acta 255 (2017) 145–152.
[36] Y. Wu, R. Zeng, J. Nan, D. Shu, Y. Qiu, S.L. Chou, Adv. Energy Mater. 7 (2017) 1700278.
[37] W. Luo, M. Allen, V. Raju, X. Ji, Adv. Energy Mater. 4 (2014) 1400554.
[38] L. Zhao, J. Zhao, Y.-S. Hu, Z. Zhou, M. Armand, L. Chen, Adv. Energy Mater. 2 (2012) 962–965.
[39] S. Renault, V.A. Mihali, K. Edström, D. Brandell, Electrochem. Commun. 45 (2014) 52–55.
[40] B. Häupler, A. Wild, U.S. Schubert, Adv. Energy Mater. 5 (2015) 1402034.
[41] S. Muench, A. Wild, C. Friebe, B. Häupler, T. Janoschka, U.S. Schubert, Chem. Rev. 116 (2016) 9438–9484.
[42] L. Zhu, J. Liu, Z. Liu, L. Xie, X. Cao, ChemElectroChem 6 (2019) 787–792.
[43] L. Mu, Y. Lu, X. Wu, Y. Ding, Y.S. Hu, H. Li, L. Chen, X. Huang, Green Energy Environ. 3 (2018) 63–70.
[44] S. Gu, S. Wu, L. Cao, M. Li, N. Qin, J. Zhu, Z. Wang, Y. Li, Z. Li, J. Chen, Z. Lu, J. Am. Chem. Soc. 141 (2019) 9623–9628.
[45] T. Huang, D. Lu, L. Ma, X. Xi, R. Liu, D. Wu, Chem. Eng. J. 349 (2018) 66–71.
[46] H. Li, M. Tang, Y. Wu, Y. Chen, S. Zhu, B. Wang, C. Jiang, E. Wang, C. Wang, J. Phys. Chem. Lett. 9 (2018) 3205–3211.
[47] Z.P. Song, T. Xu, M.L. Gordin, Y.B. Jiang, I.T. Bae, Q.F. Xiao, H. Zhan, J. Liu, D.H. Wang, Nano Lett. 12 (2012) 2205–2211.
[48] J. Manuel, X. Zhao, K.-K. Cho, J.-K. Kim, J.-H. Ahn, ACS Sustain Chem. Eng. 6 (2018) 8159–8166.
[49] S. Zhu, M. Tang, Y. Wu, Y. Chen, C. Jiang, C. Xia, S. Zhuo, B. Wang, C. Wang, Sustain. Energy Fuels 3 (2019) 142–147.
[50] W. Ai, W. Zhou, Z. Du, C. Sun, J. Yang, Y. Chen, Z. Sun, S. Feng, J. Zhao, X. Dong, W. Huang, T. Yu, Adv. Funct. Mater. 27 (2017) 1603603.
[51] J. Lee, M.J. Park, Adv. Energy Mater. 7 (2017) 1602279.
[52] G. Booth, H. Zollinger, K. McLaren, W.G. Sharpples, A. Westwell, Dyes, General Survey, Wiley-VCH Verlag GmbH & Co, Weinheim, 2000, pp. 677–729.
[53] X. Chen, H. Wang, H. Yi, X. Wang, X. Yan, Z. Guo, J. Phys. Chem. C 118 (2014) 8262–8270.
[54] T. Debashis, H.M. Viswanatha, M.N.K. Harish, S. Sampath, J. Electrochem. Soc. 167 (2020).
[55] A. Fallah-Shojaei, K. Tabatabaeian, F. Shirini, S.Z. Hejazi, RSC Adv. 4 (2014) 9509–9516.
[56] C. Guo, K. Zhang, Q. Zhao, L. Pei, J. Chen, Chem. Comm. 51 (2015) 10244–10247.
[57] Y. Hu, Y. Gao, L. Fan, Y. Zhang, B. Wang, Z. Qin, J. Zhou, B. Lu, Adv. Energy Mater. 10 (2020) 2002780.
[58] W. Tang, R. Liang, D. Li, Q. Yu, J. Hu, B. Cao, C. Fan, ChemSusChem 12 (2019) 2181–2185.
[59] L. Zhu, G. Ding, L. Xie, X. Cao, J. Liu, X. Lei, J. Ma, Chem. Mater. 31 (2019) 8582–8612.
[60] Y. Wang, Y. Ding, L. Pan, Y. Shi, Z. Yue, Y. Shi, G. Yu, Nano Lett. 16 (2016) 3329–3334.
[61] W. Deng, X. Liang, X. Wu, J. Qian, Y. Cao, X. Ai, J. Feng, H. Yang, Sci. Rep. 3 (2013) 2671.
[62] W. Xu, A. Read, P.K. Koech, D. Hu, C. Wang, J. Xiao, A.B. Padmaperuma, G.L. Graff, J. Liu, J.G. Zhang, J. Mater. Chem. 22 (2012) 4032–4039.
[63] G. Yang, F. Bu, Y. Huang, Y. Zhang, I. Shakir, Y. Xu, ChemSusChem 10 (2017) 3419–3426.
[64] L. Pérez-Lombard, J. Ortiz, D. Velázquez, Energy Effic. 6 (2013) 239–254.
[65] H. Banda, D. Damien, K. Nagarajan, A. Raj, M. Hariharan, M.M. Shaijumon, Adv. Energy Mater. 7 (2017) 1701316.
[66] J. Song, M.Z. Bazant, J. Electrochem. Soc. 160 (2013) A15–A24.
[67] J. Bisquert, G. Garcia-Belmonte, P. Bueno, E. Longo, L.O.S. Bulhões, J. Electroanal. Chem. 452 (1998) 229–234.
[68] A.S. Bondarenko, G.A. Ragoisha, in: A.L. Pomerantsev (Ed.), Progress in Chemometrics Research, Nova Science Publishers, New York, 2005, pp. 89–102.
[69] W. Wei, L. Li, L. Zhang, J. Hong, G. He, Mater. Lett. 213 (2018) 126–130.
[70] A. Lasia, Electrochem. Impedance Spectrosc. Its Appl, Springer, New York, 2014.
[71] M. Musiani, M. Orazem, B. Tribollet, V. Vivier, Electrochim. Acta 56 (2011) 8014–8022.
[72] V.A. Nikitina, A. Nazet, T. Sonnleitner, R. Buchner, J. Chem. Eng. Data 57 (2012) 3019–3025.